Thermally exfoliated graphene based counter electrode for low cost dye sensitized solar cells

Adarsh Kaniyoor and Sundara Ramaprabhu

Related Articles

Investigation of the opulent porosity for better performance of dye-sensitized solar cell
J. Renewable Sustainable Energy 5, 013112 (2013)

Photocurrent induced by two-photon excitation in ZnTeO intermediate band solar cells
Appl. Phys. Lett. 102, 052111 (2013)

Schottky-barrier solar cell based on layered semiconductor tungsten disulfide nanofilm
Appl. Phys. Lett. 101, 263902 (2012)

Application of non-metal doped titania for inverted polymer solar cells
J. Appl. Phys. 112, 123110 (2012)

Quantum-dot density dependence of power conversion efficiency of intermediate-band solar cells
J. Appl. Phys. 112, 124515 (2012)

Additional information on J. Appl. Phys.

Journal Homepage: http://jap.aip.org/
Journal Information: http://jap.aip.org/about/about_the_journal
Top downloads: http://jap.aip.org/features/most_downloaded
Information for Authors: http://jap.aip.org/authors

Thermally exfoliated graphene based counter electrode for low cost dye sensitized solar cells

Adarsh Kaniyoor and Sundara Ramaprabhu[a)]

Alternative Energy and Nanotechnology Laboratory, Nano Functional Materials Technology Centre, Department of Physics, Indian Institute of Technology Madras, Chennai, India.

Graphene obtained from thermal exfoliation of graphite oxide are highly wrinkled and have large surface area. Their wrinkled nature is expected to give them excellent catalytic activity. Herein, we demonstrate the use of thermally exfoliated graphene (TEG) as cost effective electrocatalyst for the tri-iodide reduction in dye sensitized solar cells (DSSCs). X-ray diffraction, Raman and Infra red spectroscopy and electron microscopy studies confirm the defective and wrinkled nature of TEG. BET surface area measurement show a large surface area of $\sim$ 470 m^2/g. The counter electrode was fabricated by drop casting a slurry of TEG dispersed in a Nafion:Ethanol solution on fluorine doped tin oxide (FTO) substrates. The use of Nafion prevented film "peel off," thus ensuring a good substrate adhesion. Electrochemical impedance spectroscopy reveals that TEG had a catalytic performance comparable to that of Pt, suggesting its use as counter electrode material. As expected, the DSSC fabricated with Nafion solubilized TEG/FTO as counter electrode shows an efficiency of about 2.8%, comparable to Pt counter electrode based DSSC which has an efficiency of about 3.4%. © *2011 American Institute of Physics*. [doi:10.1063/1.3600231]

I. INTRODUCTION

The counter electrodes (CEs) in dye sensitized solar cells (DSSCs) have a dual role. They not only act as current (electronic charge) collectors but also catalyze the reduction of tri-iodide species to iodide species which ensures the continuous working of the cell.[1] Platinum (Pt) is the conventional choice for counter electrodes due to its high catalytic activity and high corrosion resistance to iodine in the electrolyte.[1–4] However, since Pt is an expensive noble metal, alternate counter electrode materials with good catalytic activity and corrosion resistance are necessary. Several carbon based materials like graphite,[5] amorphous carbon (carbon black, nano and micro carbon etc),[6–8] carbon nanotubes (single walled,[9] double walled,[10] multi walled[11]) have been employed as counter electrodes and substantial efficiencies have been obtained. Graphene,[12] the newly discovered 2D form of carbon is also expected to significantly improve the performance of DSSCs.

Graphene has received significant attention over the past few years owing to its excellent electrical and catalytic properties. The synthesis and use of strictly single layer graphene presents difficulties and challenges. Hence, attempts are now focused on the use of exfoliated graphene consisting of a few layers (2–3 or even up to 10).[13] These structures can be synthesized in large quantities via a variety of techniques namely thermal exfoliation,[14] vacuum exfoliation,[15] chemical exfoliation,[16] etc. These methods are based on the harsh oxidation of graphite to graphite oxide followed by its simultaneous reduction and exfoliation. Among these methods, graphene obtained by thermal exfoliation technique seems to the best due to its low oxygen content and higher surface area. Graphene based counter electrodes are expected to decrease the charge transfer resistance due to their good conductivity, high surface area, and high catalytic activity. The decrease in charge transfer resistance would increase the exchange current density, thereby improving the overall efficiency. There are a few reports on the use of graphene as counter electrode. Hong *et al.*[17] reported that graphene/PEDOT:PSS transparent counter electrode based DSSC had an efficiency of $\sim$4.3%. This was $\sim$0.71 times the efficiency of their Pt based DSSC, which had an efficiency of $\sim$6.3%.

In this work, we demonstrate the use of Nafion solubilized thermally exfoliated graphene (TEG) as counter electrode material for DSSCs. The use of Nafion, a binder ensures a firmly adhered film, resulting in good efficiency. No other functionalization procedure has been carried out on graphene. The cell prepared using graphene based counter electrode (Fig. 1) showed high energy conversion efficiency, almost comparable to our Pt based reference cell and is thus a considerable improvement over the previous report.

II. EXPERIMENTAL SECTION

Natural flake graphite (99.99%, 10 mesh) was purchased from Alfa Aesar, U.S.A. P25 TiO$_2$ was obtained from Degussa, Germany. FTO conducting plates (TEC 22-7, TEC 22-15), SX1170-25 spacer, Pt catalyst Plastisol, and Ruthenium 535 bis-TBA (N719) dye were purchased from Solaronix, Switzerland. LiI was purchased from Merck. 5% Nafion solution was obtained from Dupont. All other reagents used were purchased from Sigma Aldrich or Alfa Aesar.

TEG was synthesized in two stages. First, graphite oxide (GO) was prepared from graphite (Gr) following modified Hummers' method.[18] Thermal exfoliation was carried out as reported by Schniepp *et al.*[14] A small quantity of GO was

---

[a)]Author to whom correspondence should be addressed. Electronic mail: ramp@iitm.ac.in.
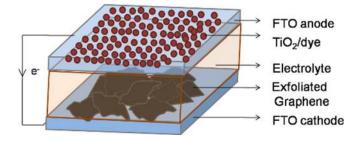
FIG. 1. (Color online) Schematic of thermally exfoliated graphene counter electrode based DSSC.

taken in a quartz boat and introduced into a preheated (1050 °C) tubular furnace. An inert atmosphere of Ar was maintained inside the quartz tube during exfoliation. Exfoliation occurred within 30 s. The resulting exfoliated graphene was dispersed in a solution consisting of Nafion and ethanol in the ratio 1:1 by vol. The dispersion was ultrasonicated for 1 h to obtain a homogeneous dark solution. Few drops of the above dispersion were dropped onto masked FTO plates (TEC 22-7, 7 Ω/sq.). The geometrical area was maintained at ~ 0.36 cm^2. The FTO plates were pre-cleaned by rinsing with soap water and de-ionized water, followed by ultrasonication in acetone and ethanol bath for 15 min each.

The TiO$_2$ paste formulation was based on Pechini type sol-gel method as developed by Krasovec et al.[19] The resultant paste was spread on to FTO plates (TEC 22-15, 15 Ω/sq) using a glass rod. The dimensions and thickness were controlled using a framework of Scotch 3M tape. The coatings were finally sintered at 450 °C in a furnace for 1 h. The active area of the photo anode was ~ 0.25 cm^2. The TiO$_2$ film was immersed in the dye solution for ~ 24 h for complete dye uptake. The dye solution consisted of 0.5 mM of Ru(2,2′-bipyridyl-4,4′-dicarboxylic acid)$_2$(NCS)$_2$:2(tetrabutylammonium), commonly known as the (N719) dye in a 1:1 solution of acetonitrile: t-butyl alcohol. The TiO$_2$ photoelectrode and the graphene counter electrodes were clamped with a SX 1170-25 film as spacer, cut into appropriate size and shape. The space between the electrodes was filled with an electrolyte consisting of 0.5 M LiI, 0.05 M I$_2$, 0.5 M TBP in acetonitrile and valeronitrile (85:15 by vol).

X-ray diffraction was carried out using a PANalytical X'PERT Pro X-ray diffractometer with nickel-filtered Cu K$_\alpha$ radiation as the X-ray source. The pattern was recorded in the 2θ range of 5° to 90° with a step size of 0.016°. The Raman spectra were obtained with a WITEC alpha 300 Confocal Raman system equipped with a Nd:YAG laser (532 nm) as the excitation source. The intensity was kept at minimum to avoid laser induced heating. FTIR spectra were analyzed via a Perkin Elmer FTIR spectrometer in the range 500–4000 cm^{-1}. BET measurement was carried out using Micromeritics ASAP 2020 V3.01 G surface area analyzer. The morphology of the samples was characterized by field emission scanning electron microscopy (FESEM, FEI QUANTA). Transmission electron microscopy (TEM) was carried out using a JEOL JEM-2010 F microscope. For TEM measurements, the graphene powder was dispersed in absolute ethanol using mild ultrasonication and casted onto carbon coated Cu grids (SPI supplies). Electrochemical

impedance measurements were carried out in the frequency range 100 kHz to 0.1 Hz using Solartron 1400 and 1470E Cell Test System. The I-V measurements of the fabricated solar cells were measured under AM 1.5 G solar radiation using a Newport 150 W Class A Solar Simulator attached with Keithley 2420 source meter. The intensity was calibrated to give an output of 1 Sun (100 mW/cm^2) using a thermopile detector and also using a NREL calibrated Si reference cell. EDX (energy dispersion by x-rays) analysis was carried out to determine the elemental composition. The EDX spectra were noted at six different places and averaged to get the final value. Electrical conductivity measurements were done using linear four probe method.

III. RESULTS AND DISCUSSION

Figure 2(a) shows the FT-IR spectra of the parent graphite, oxidized GO and TEG. The graphite precursor shows a broad peak centered at 3440 cm^{-1} corresponding to the vibrations of water molecules. These signals may belong to adsorbed water or –OH in carboxylic groups resulting due to some pretreatment given prior to purchase. The doublet peaks at 2922 cm^{-1} and 2860 cm^{-1} correspond to symmetric and antisymmetric stretching vibrations of –CH$_2$.[25] While graphite can be used as a counter electrode material, GO cannot be used due to the presence of large number of oxygen containing functional groups which makes it non-conducting. In GO, the peaks corresponding to water molecules are broad, indicating the presence of large quantities of adsorbed water.[26] Peaks corresponding to the C=O and C–O stretching vibrations of COOH groups can be seen at 1720 cm^{-1} and 1225 cm^{-1}.[20] The presence of these oxygen containing functional groups suggests that graphite oxide is a highly oxidized system. After high temperature exfoliation, the –OH functional groups are removed to a great extent indicated by the reduction in intensity of the –OH peaks in TEG. Other peaks like CH$_2$ (2922 cm^{-1} and 2860 cm^{-1}) and the peaks at 1720 cm^{-1}, 1225 cm^{-1} and 1050 cm^{-1} corresponding to C=O, and C–O groups are present but are broadened. The reappearance of some of these groups suggests a partial restoration of the carbon basal planes after exfoliation.[27]

Figure 2(b) represents the Raman spectra of pristine Gr, GO, and TEG. In order to avoid laser induced damage, the intensity of the laser was maintained as low as possible during the experiment. Graphite shows a sharp peak at ~ 1585 cm^{-1}, corresponding to the optically allowed E_{2g} phonon vibrations. This peak is a characteristic of all sp^2 hybridized carbons and is called the G band.[22] The disorder induced band (D band) can be found at ~ 1350 cm^{-1} with a very low intensity, suggesting that the graphite used is nearly defect free. Defects at the edge of graphite sheets can also contribute to the D band. The 2 D band, also known as the G′ band is centered at ~ 2720 cm^{-1}. The G band in the case of GO and TEG occur at ~ 1609 cm^{-1} and at ~ 1605 cm^{-1}, respectively. Also, a broadening of G band is observed in GO and EG, which can be attributed to an increase in the disorder resulting from the rigorous oxidation treatments. This disorder is also visible in the form of highly broadened and intense D band, both in GO and EG. The ratio between the
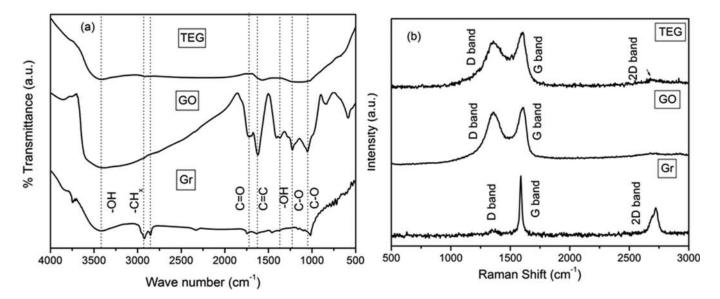
FIG. 2. (a) FT-IR spectra of graphite (Gr), graphite oxide (GO) and graphene (TEG) shows the presence of large amount of –OH groups in GO which are removed considerably, upon exfoliation. (b) Raman spectra of graphite (Gr), graphite oxide (GO) and graphene (EG) indicate the presence of large amount of defects and a partial restoration of basal planes in graphene.

intensities of the D and G bands is generally used to predict the presence of defects and the size of the in-plane sp^2 domain.[23] The ratio of peak intensities of D and G-mode (I_D/I_G) for HEG is around 0.85 as compared to 0.99 for GO. This indicates that a good restoration of π-conjugated structure occurs upon exfoliation due to a "self healing" mechanism.[24]

On conversion of graphite to graphene, the long range order of graphite is destroyed. The XRD patterns of Gr, and EG, presented in Fig. 3 clearly prove this transformation. The intense peak occurring at ~26.5° in Gr correspond to the (002) plane and has a d-spacing of 0.34 nm. This characteristic peak of hexagonal graphite indicates the presence of long range order in the sample thus confirming of its crystalline nature. Upon conversion of Gr into GO the peak position shifts to 10.5° (Ref. 20) and the interlayer spacing increases to 0.84 nm. This increase in d-spacing is due to the intercala-

tion of -OH containing functional groups in between the graphene layers. After exfoliation at 1050 °C, all crystalline peaks disappear and a broad peak appears starting from ~15° to 30°.[21] The interlayer spacing decreases to 0.37 nm which suggests that the removal of oxygen and water from the layers occur to a large extent. This broadening also suggests the destruction of long range order in graphene.

BET surface area measurements were carried out to determine the surface area of the as grown powdered graphene. The N$_2$ adsorption desorption isotherm for EG is presented in Fig. 4. The isotherm exhibits type-II pattern and type H3 hysterisis loop. According to certain reports, the presence of adsorption hysteresis suggests that the isotherm is a pseudo type-II pattern.[28] Generally, this kind of behavior is observed due to multi layer adsorption in materials having
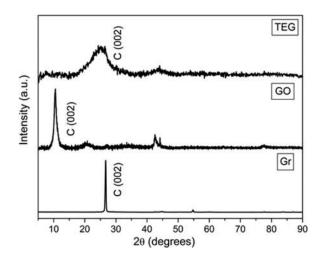

FIG. 3. Powder X-ray diffractograms of graphite (Gr), graphite oxide (GO) and exfoliated graphene (TEG). The amorphous like peak in graphene suggest the destruction of long range crystalline order.
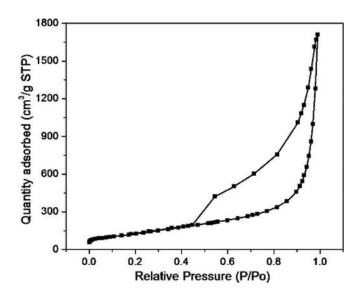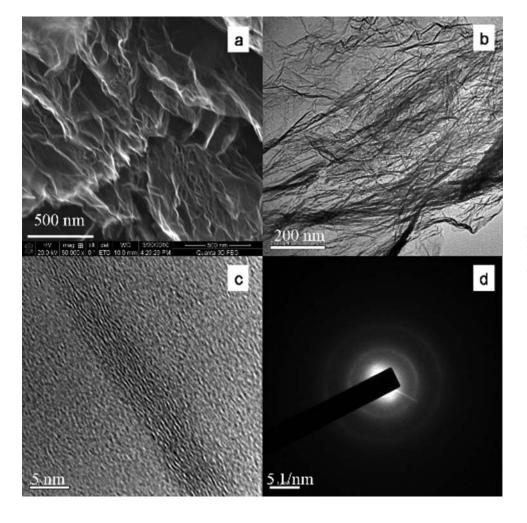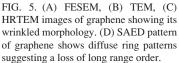

FIG. 4. Nitrogen adsorption desorption isotherm of exfoliated graphene. The BET surface area was calculated from the above graph using the BET equation.

FIG. 5. (A) FESEM, (B) TEM, (C) HRTEM images of graphene showing its wrinkled morphology. (D) SAED pattern of graphene shows diffuse ring patterns suggesting a loss of long range order.

slit like pores or aggregates of platy particles. In exfoliated graphene, adsorption occurs on the surface of the graphene sheets but due to their few layered structure, slit like open pores exist. These open pores are responsible for hysteresis loop observed in graphene materials.[15] From the linear region of the graph and using the BET equation, the BET surface area was determined to be $\sim$470 m^2/g.

The electron microscopy images of graphene are presented in Fig. 5. The effect and extent of exfoliation is clearly visible in the FESEM image of graphene in Fig. 5(a). The sheets appear to be uniformly exfoliated. The separation induced between the graphitic layers during exfoliation is due to the removal of oxygen and water from graphite oxide. This gives a fluffy morphology to the as grown graphene powder. The real nature of the graphene sheets becomes clear in the TEM image (Fig. 5(b)). A large number of wrinkles can be seen on graphene sheets. The presence of these wrinkles in a characteristic of exfoliated graphene and is probably due to the various functional groups like the epoxides present on the basal planes. The HRTEM image (Fig. 5(c)) of an overlapped region shows the layers of graphene. Selected area electron diffraction (SAED) was performed on the graphene sheets and the corresponding SAED pattern is shown in Fig. 5(d). The SAED pattern show only weak and diffuse rings, indicating the loss of long range ordering in the graphene sheets.[29]

In order to evaluate the catalytic activity of TEG, electrochemical impedance measurements were carried out (Fig. 6). The measurements were carried out in a symmetric cell configuration with the same electrolyte as in the actual cell. Impedance measurements were also carried out on Pt counter electrode for comparison purposes. In both the cases a
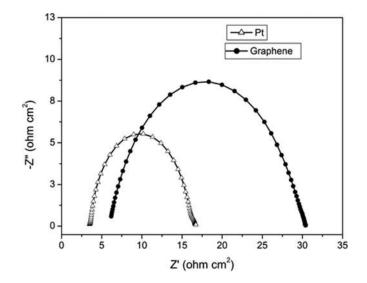

FIG. 6. Nyquist plots of graphene and Pt in a symmetric cell configuration showing a comparable electrochemical behavior.
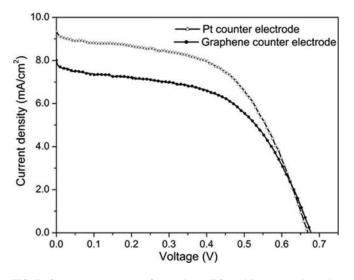
FIG. 7. Current voltage curves for graphene (EG) and Pt counter electrodes based DSSCs obtained using AM 1.5 solar illumination with an intensity of 1 sun.

similar pattern was obtained indicating a similar electrochemical behavior of TEG and Pt. However, as expected both the sheet resistance and charge transfer resistance were slightly higher in the case of TEG. The series resistances (normalized with respect to area) were 3.5 Ωcm^2 and 6.2 Ωcm^2 and the charge transfer resistance (R_{ct}) values were 6.5 Ωcm^2 and 11.7 Ωcm^2 for Pt and TEG, respectively. Though the R_{ct} values were slightly higher compared to Pt, it is still very low compared to reported values for graphite.[30] This suggests that a thick film of wrinkled or defective graphene promotes the electron-transfer kinetics at the counter electrode-electrolyte interface, resulting in its relatively low charge-transfer resistance.

The current-voltage curve of EG counter electrode based DSSC is given in Fig. 7. For reference, the I-V curve for Pt counter electrode based DSSC is also presented. For the reference cell, the parameters open circuit voltage (V_{oc}), current density (J_{sc}), fill factor (FF) and efficiency (η) are as follows: 0.67 V, 9.1 mA/cm^2, 0.55 and 3.37%. Corresponding values for the graphene based DSSC are 0.68 V, 7.7 mA/cm^2, 0.54, 2.82%. The current density in the case of TEG is lower than that of Pt. This decrease can be attributed to an increase in the series resistance (R_s) in EG based DSSCs. This is also corroborated by impedance measurements in Fig. 6, which shows a small increase in series resistance in EG based cell. These changes can directly lead to a decrease in the current density according to the Eq. (30)

$$J_{sc} = J_{ph} - J_o.exp[(q.J_{sc}.R_s/nkT) - 1] - J_{sc}.R_s/R_{sh}, \quad (1)$$

where J_{ph} and J_o are the photocurrent and reverse saturation current and n is the ideality factor. This could be a possible reason for the decrease in current density in the case of graphene. Nevertheless, the efficiency of graphene based DSSC is around 0.83 times the efficiency of the Pt based DSSC which is higher than that reported in the literature. The comparable performance of graphene based DSSC can be attributed to its high surface area and reasonable catalytic activity toward the reduction of tri-iodide.

To further understand the role of TEG as efficient counter electrode material, elemental analysis and electrical conductivity measurements were carried out. TEG obtained from the reduction of GO has some amount of functional groups even after exfoliation. The presence of these functional groups affects the electrical conductivity of the samples, which in turn would affect the series resistance of the cell. Schniepp et al.[14] have showed that the lowest amount of oxygen content was obtained when exfoliation was done at 1050 °C. In the present samples, EDX measurements showed an oxygen content (by weight) of $\sim$37% in GO and $\sim$9% in TEG, which is in conformity with the results of Schniepp et al. The electrical conductivity measurements on GO and TEG, revealed a value of $\sim 6.65 \times 10^{-4}$ S/m and 3.95×10^2 S/m, respectively. As can be seen the conductivity increases sharply by an order of 10^6 when GO is reduced to TEG. Exfoliation done at lower temperature (<1050 °C) would only result in higher oxygen content and lower electrical conductivity. This would decrease the overall power conversion efficiency. In addition, it should be noted that graphite has very low oxygen content and a high electrical conductivity, but the charge transfer resistance offered by it is large. This suggests that some amount of oxygen containing functional groups is required to achieve an optimum performance in DSSCs. Therefore, thermally exfoliated graphene (at 1050 °C) appears to ideal as a counter electrode material for DSSCs.

IV. CONCLUSION

The synthesis and use of thermally exfoliated graphene as a novel counter electrode electrocatalyst material for tri-iodide reduction in DSSCs is demonstrated. Due to its high surface area and defect rich surface, graphene shows relatively low charge transfer resistance and hence a photovoltaic performance comparable to that of Pt based DSSC is obtained. Since exfoliated graphene can be synthesized in large quantities at very low costs, exfoliated graphene is a good alternative for Pt counter electrodes in DSSCs.

[1]T. N. Murakami, and M. Grätzel, Inorg. Chim. Acta **361**, 572 (2008).
[2]B. O'Regan, and M. Grätzel, Nature **353**, 737 (1991).
[3]C. H. Yoon, R. Vittal, J. Lee, W.-S. Chae, and K.-J. Kim, Electrochim. Acta **53**, 2890 (2008).
[4]S. R. Gajjela, K. Ananthanarayanan, C. Yap, M. Grätzel, and P. Balaya, Energy Environ. Sci. **3**, 838 (2010).
[5]J. Chen, K. Li, Y. Luo, X. Guo, D. Li, M. Deng, S. Huang, and Q. Meng, Carbon **47**, 2704 (2009).
[6]E. Ramasamy, W. J. Lee, D. Y. Lee, and J. S. Song, Appl. Phys. Lett. **90**, 173103 (2007).
[7]Z. Huang, X. Liu, K. Li, D. Li, Y. Luo, H. Li, W. Song, L. Q. Chen, and Q. Meng, Electrochem. Commun. **9**, 596 (2007).
[8]T. N. Murakami, S. Ito, Q. Wang, M. K. Nazeeruddin, T. Bessho, I. Cesar, P. Liska, R. H. Baker, P. Comte, P. Péchy, and M. Grätzel, J. Electrochem. Soc. **153**, A2255 (2006).
[9]B. Ahmmad, Y. Kusumoto, M. Abdulla-Al-Mamun, A. Mihata, and H. Yang, J. Sci. Res. **1**, 430 (2009).

[10]D. W. Zhang, X. D. Li, S. Chen, F. Tao, Z. Sun, X. J. Yin, and S. M. Huang, J. Solid State Electrochem. **14**, 1541 (2009).

[11]W. J. Lee, E. Ramasamy, D. Y. Lee, and J. S. Song, ACS Appl. Mater. Interfaces **1**, 1145 (2009).

[12]K. S. Novoselov, A. K. Geim, S. V. Morozov, D. Jiang, Y. Zhang, S. V. Dubonos, I. V. Grigorieva, and A. A. Firsov, Science **306**, 666 (2004).

[13]C. N. R. Rao, A. K. Sood, K. S. Subrahmanyam, and A. Govindaraj, Angew. Chem. Int. Ed **48**, 7752 (2009).

[14]H. C. Schniepp, J. L. Li, M. J. McAllister, H. Sai, M. Herrera- Alonso, D. H. Adamson, R. K. Prud'homme, R. Car, D. A. Saville, and I. A. Aksay, J. Phys. Chem. B **110**, 8355 (2006).

[15]L. Wei, T. Dai-Ming, H. Yan-Bing, Y. Cong-Hui, S. Zhi-Qiang, C. Xue- Cheng, C. Cheng-Meng, H. Peng-Xiang, L. Chang, and Y. Quan-Hong, ACS Nano **3**, 3730 (2009).

[16]S. Stankovich, D. A. Dikin, R. D. Piner, K. A. Kohlhaas, A. Klein- hammes, Y. Jia, Y. Wu, S. T. Nguyen, and R. S. Ruoff, Carbon **45**, 1558 (2007).

[17]W. Hong, Y. Xu, G. Lu, C. Li, and G. Shi, Electrochem. Commun. **10**, 1555 (2008).

[18]X. Sun, Z. Liu, K. Welsher, J. T. Robinson, A. Goodwin, S. Zaric, and H. Dai, Nano Res. **1**, 203 (2008).

[19]U. O. Krasovec, M. Berginc, and M. Hocevar, Sol. Energy Mater. Sol. Cells **93**, 379 (2009).

[20]H.-K. Jeong, L. Colakerol, M. H. Jin, P.-A. Glans, K. E. Smith, and Y. H. Lee, Chem. Phys. Lett. **460**, 499 (2008).

[21]H.-L. Guo, X.-F. Wang, Q.-Y. Qian, F.-B. Wang, and X.-H. Xia, ACS Nano **3**, 2653 (2009).

[22]S. Reich, C. Thomsen, Phil. Trans. R. Soc. Land. A **362**, 2271 (2004).

[23]F. Tuinstra and J. L. Koenig, J. Chem. Phys. **53**, 1126 (1970).

[24]G. Wang, J. Yang, J. Park, X. Gou, B. Wang, H. Liu, and J. Yao, J. Phys. Chem. C **112**, 8192 (2008).

[25]K. A. Worsley, P. Ramesh, S. K. Mandal, S. Niyogi, M. E. Itkis, and R. C. Haddon, Chem. Phys. Lett. **445**, 51 (2007).

[26]G. I. Titelma, V. Gelman, S. Bron, R. L. Khalfin, Y. Cohen, and H. Bianco-Peled, Carbon **43**, 641 (2005).

[27]G. Wang, B. Wang, J. Park, J. Yang, X. Shen, and J. Yao, Carbon **47**, 68 (2009).

[28]K. S. W. Sing, J. Porous Mater. **2**, 5 (1995).

[29]J. Liu, H. Jeong, J. Liu, K. Lee, J.-Y. Park, Y. H. Ahn, and S. Lee, Carbon **48**, 2282 (2010).

[30]S. Gagliardi, L. Giorgi, R. Giorgi, N. Lisi, T. D. Makris, E. Salernitano, and A. Rufoloni, Superlattice Microst. **46**, 205 (2009).